Charge transfer emission between π- and 4f-orbitals in a trivalent europium complex

Check for updates

Yuichi Kitagawa [1,2,8] ✉, Toranosuke Tomikawa[3,8], Kota Aikawa[3], Shiori Miyazaki[4], Tomoko Akama[2], Masato Kobayashi[2,5], Mengfei Wang[2], Sunao Shoji[6], Koji Fushimi[1], Kiyoshi Miyata[4], Yuichi Hirai[7], Takayuki Nakanishi[7], Ken Onda[4], Tetsuya Taketsugu[2,5] & Yasuchika Hasegawa[1,2] ✉

Photoinduced metal-to-ligand (or ligand-to-metal) charge-transfer (CT) states in metal complexes have been extensively studied toward the development of luminescent materials. However, previous studies have mainly focused on CT transitions between d- and π-orbitals. Herein, we report the demonstration of CT emission from 4f- to π-orbitals using a trivalent europium (Eu(III)) complex, supported by both experimental and theoretical analyses. The Eu(III) complex exhibits an eight-coordination structure, comprising three anionic nitrates and two neutral electron-donating ligands containing a carbazole unit. The diffuse reflectance spectrum of the complex displays an absorption band at 440 nm and time-resolved emission analyses reveal a characteristic emission band at 550 nm. Comparative studies employing a trivalent gadolinium (Gd(III)) complex, alongside quantum chemical analyses, confirm that the observed absorption and emission bands are associated with CT transitions between π- and 4f-orbitals. The observation of CT emission based on the 4f-orbital offers novel insights into the field of molecular luminescence science and technology.

Metal complexes are organic–inorganic hybrid compounds that have been widely used in the fabrication of molecular photofunctional materials, such as photosensitizers[1,2], luminophores[3,4], and photocatalysts[5,6]. Controlling the photoinduced charge transfer (CT) between metals and organic ligands is key to their photofunctionality. Numerous transition metal complexes reportedly exhibit prominent photofunctionality due to ligand-to-metal charge transfer (LMCT) or metal-to-ligand charge transfer (MLCT)[7–9]. Kinoshita successfully constructed a wide-band (~1000 nm) sensitized solar cell based on the MLCT excited states of ruthenium complexes[7]. Recently, Bauer suggested dual emission from 3d-orbital-based LMCT and MLCT states using an Fe(III) complex[8]. Zhang successfully constructed a Zr(IV) complex with long-lived LMCT excited states, featuring strong emission, and verified its applicability as an effective photoredox catalyst[9]. Previous research has expanded the application scope of CT excitons in various metal complexes; however, the investigation of CT excitons has been limited to the d-orbital. The properties of CT excitons are closely linked to the characteristics of the transition orbitals. Investigating unexplored CT excitons is essential for the development of new photo-functional metal complexes.

Herein, we focused on the CT excited state between the 4f- and π-orbitals in trivalent lanthanide (Ln(III)) complexes (Fig. 1a). The first study on the CT excited states of lanthanide complexes was reported by Jørgensen in 1962[10]. He observed a broad absorption band in the visible region for a trivalent europium (Eu(III)) complex with dithiocarbamate ligands, which was assigned to the CT transition from the π- to 4f-orbital. This Eu(III) complex exhibited the lowest redox potential ([Eu(III)/Eu(II) = −0.35 V vs. NHE])[11] among trivalent lanthanides and formed a low-energy CT level based on the 4f-orbital. Following this groundbreaking observation, subsequent studies have been conducted on CT excited states between the 4f- and π-orbitals for exploring phenomena, such as absorption and 4f-4f emission quenching, the photosensitization effect, and investigating perturbation effects on the chiroptical properties of Eu(III) complexes[12–26]. The demonstration of CT emission based on a combined experimental and theoretical study will open new scientific avenues for the development of photofunctional metal complexes.

To demonstrate CT emission from 4f- to π-orbitals, we designed an eight-coordinate Eu(III) complex (Fig. 1b, [Eu(NO₃)₃(MCPO)₂], **Eu-MCPO**). An electron-donating neutral ligand, (3,6-dimethoxy-9H-

¹Faculty of Engineering, Hokkaido University, Kita 13, Nishi 8, Kita-ku, Sapporo, Hokkaido, 060–8628, Japan. ²Institute for Chemical Reaction Design and Discovery (WPI-ICReDD), Hokkaido University, Kita 21, Nishi 10, Kita-ku, Sapporo, Hokkaido, 001-0021, Japan. ³Graduate School of Chemical Sciences and Engineering, Hokkaido University, Kita 13, Nishi 8, Sapporo, Hokkaido, 060-8628, Japan. ⁴Department of Chemistry, Kyushu University, 744 Motooka, Nishi, Fukuoka, 829-0395, Japan. ⁵Faculty of Science, Hokkaido University, Kita 10, Nishi 8, Kita-ku, Sapporo, Hokkaido, 060-0810, Japan. ⁶Faculty of Engineering, Nara Women's University, Kitauoya-Nishimachi, Nara, 630-8506, Japan. ⁷National Institute for Materials Science, 1-1 Namiki, Tsukuba, Ibaraki, 305-0044, Japan. ⁸These authors contributed equally: Yuichi Kitagawa, Toranosuke Tomikawa. ✉e-mail: y-kitagawa@eng.hokudai.ac.jp; hasegaway@eng.hokudai.ac.jp
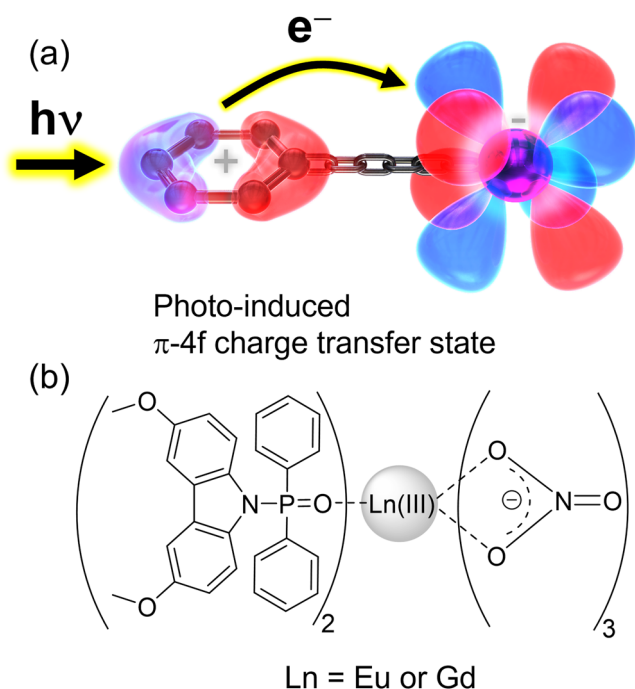
Fig. 1 | Charge transfer state and chemical structures. a Schematic image of photo-induced charge transfer state between the 4f- and π-orbitals. **b** Molecular structures of **Eu-MCPO** and **Gd-MCPO**.
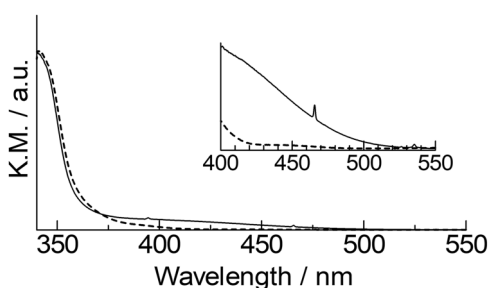

Fig. 2 | Diffuse reflectance spectra. Diffuse reflectance spectra of solid state **Eu-MCPO** (black solid line) and **Gd-MCPO** (black broken line). The weak absorption peak at approximately 465 nm corresponds to the $^7F_0 \rightarrow {}^5D_2$ transition for Eu(III).

carbazol-9-yl)diphenyl phosphine oxide (MCPO), was designed to form a CT excited energy level based on the 4f-orbital lower than the localized π-π* excited energy level. The formation of a low-energy level is essential for suppressing the relaxation process from the CT excited state to the ligand-localized excited state. An anionic nitrate ligand with low steric hindrance was selected for the formation of stable coordination structures. The photophysical properties of the eight-coordinate Gd(III) complex ([Gd(NO₃)₃(MCPO)₂], **Gd-MCPO**, Fig. 1b) and nine-coordinate Eu(III) complex ([Eu(NO₃)₃(MCPO)₂(H₂O)], **Eu-MCPO-H₂O**, Fig. S1) were also evaluated for the comparison of the CT transition properties. The CT emission properties were analyzed by steady and time-resolved emission spectroscopy. Quantum chemical calculations were performed to investigate the electronic structures of the CT excited states.

Results and discussion
Structural analysis
Steric structures of **Ln-MCPO** and **Ln-MCPO-H₂O** (Ln = Eu or Gd) were analyzed by X-ray crystallography and quantum chemical calculations. **Eu-MCPO-H₂O** was found to possess a triclinic crystal system, with space group P-1 (for crystallographic data, see Fig. S6 and Table S1). We observed that the coordination site in the Eu(III) complex comprises three bidentate

nitric ligands, two phosphine oxide ligands, and one water molecule. The bidentate nitric acid and MCPO ligands have average Eu−O (NO₃) and Eu–O (MCPO) distances of 2.498 and 2.368 Å, respectively. We prepared **Eu-MCPO** by the elimination of H₂O from **Eu-MCPO-H₂O** toward the formation of the stabilized CT excited states between the 4f- and π-orbitals[24]. The PXRD pattern of dehydrated **Eu-MCPO** is different from that of **Eu-MCPO-H₂O** (Fig. S7). The **Eu-MCPO** structure optimized using quantum chemical calculations (Supplementary Note 1, Fig. S8a) demonstrates a shorter distance between the Eu(III) center and coordination oxygen atoms [average Eu−O (NO₃): 2.474 Å, average Eu–O (MCPO): 2.321 Å] than the **Eu-MCPO-H₂O** structure (For the optimized structure of **Eu-MCPO-H₂O** (Fig. S8b), the bidentate nitric acid and MCPO ligands have average Eu–O (NO₃) and Eu–O (MCPO) distances of 2.482 and 2.386 Å, respectively.). The PXRD pattern of **Gd-MCPO** was almost the same as that of **Eu-MCPO** (Fig. S7), indicating the presence of a similar crystal structure independent of the type of lanthanide ions. Thus, a comparative photophysical study using **Gd-MCPO** is reasonable for investigating the CT excited state between the 4f- and π-orbitals in **Eu-MCPO**.

Photophysical properties
The diffuse reflectance spectra of **Eu-MCPO** and **Gd-MCPO** are shown in Fig. 2. The absorption bands at 340 nm (29,400 cm⁻¹) for **Eu-MCPO** were assigned to singlet π−π* transitions of the MCPO ligands, which agree with the absorption spectrum of **Gd-MCPO**. We also observed additional absorption bands at approximately 440 nm (22,700 cm⁻¹) for **Eu-MCPO**, which were not observed for **Gd-MCPO** (Fig. 2, inset). Quantum chemical calculations were performed to determine the origin of the characteristic absorption band observed in the **Eu-MCPO** spectrum. According to the calculations, in the **Eu-MCPO** spectrum, the absorption bands in the visible region originated in the CT transition from the MCPO ligand to the Eu(III) ion (Table S2, Fig. S9). The analysis of atomic contributions to molecular orbitals indicates minimal mixing between the π-orbital and the 4f-orbital of Eu(III) (Table S3). In addition, the occupied π- and unoccupied 4f-orbitals exhibit slight mixing with the NO₃ orbitals. These findings suggest that the NO₃ orbitals may also contribute to the CT transition. The absorption coefficient at the CT absorption band is relatively low (ε < 10 cm⁻¹ M⁻¹, Fig. S10), which is correlated with the calculated small oscillator strength for the CT transition (f = 0.0019, Table S2). This low transition probability is likely due to the minimal orbital overlap between the 4f- and π-orbitals mediated by the phosphine oxide spacer.

To gain a more detailed understanding of the CT states in **Eu-MCPO**, cyclic voltammetry measurements were conducted (Fig. S11). The first oxidation potential was determined to be 0.97 V, closely matching that of the free MCPO ligand (Fig. S12, 1.00 V). Quantum chemical calculations also indicate that the observed oxidation potential corresponds to the MCPO cation (Table S4). Distinct redox waves were not observed in the voltammograms, and the reduction potential of the Eu(III) ion could not be determined; however, quantum chemical calculations suggest that the first reduction potential mainly corresponds to Eu(II) (Table S4). The π−π* and CT absorption bands of the eight-coordinate **Eu-MCPO** were found to be blue-shifted and red-shifted, respectively, compared to those of the nine-coordinate **Eu-MCPO-H₂O** (Tables S5 and S6, Figs. S13 and S14). This shift indicates a change in MCPO ligand orientation and the formation of stable CT excited states upon the elimination of H₂O. The stabilization of the CT excited state by reducing the coordination number is consistent with previously reported phenomena[24], according to which this phenomenon is ascribed to enhanced interaction between the Eu(III) ion and the organic ligand due to the reduced coordination bonding distance. The results of quantum chemical calculation with the solvent effect suggest that the stable CT excited states of **Eu-MCPO** were also formed in the solution state (Figs. S15 and S16, Tables S7 and S8) (Unfortunately, emission properties of **Eu-MCPO** in solution state cannot be estimated experimentally because of poor photo-stability (Supplementary Note 3–4, Figs. S25–S32).).

Eu-MCPO shows sharp emission bands at approximately 580, 590, 610, 635, and 700 nm, which correspond to the $^5D_0 \rightarrow {}^7F_0$, $^5D_0 \rightarrow {}^7F_1$,
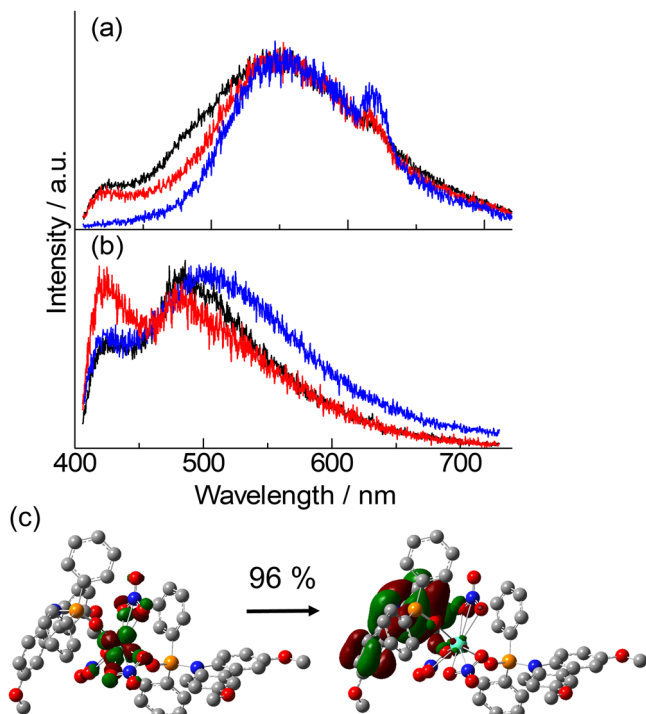
Fig. 3 | Time-resolved emission spectra and transition orbital. Time-resolved emission spectra (λ_{ex} = 368 nm) of solid-state **a** Eu-MCPO and **b** Gd-MCPO at 100 K (**a**, black line: 0–0.5 ns, red line: 0.5–1.0 ns, blue line: 2.0–3.0 ns, **b** black line: 0–0.5 ns, red line: 0.5–1.0 ns, blue line: 5.0–44 ns). Normalized by intensity maxima. **c** Results of the transition orbital analysis from the CT excited to ground state at the structure with large oscillator strength appeared during the structural relaxation using quantum chemical calculations (Fig. S21). Gray spheres represent carbon; red spheres, oxygen; blue spheres, nitrogen; orange spheres, phosphorus; and green spheres, europium.
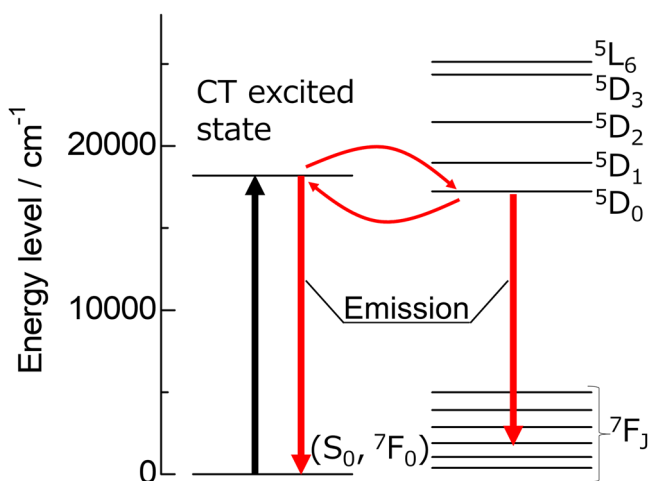

Fig. 4 | Energy diagram. Energy diagram and proposed emission mechanism for Eu-MCPO.

$^5D_0 \rightarrow {}^7F_2$, $^5D_0 \rightarrow {}^7F_3$, and $^5D_0 \rightarrow {}^7F_4$ transitions, respectively (Fig. S17, 100 K). The time-resolved emission spectra were also measured for **Eu-MCPO** and **Gd-MCPO** (Fig. 3). The **Eu-MCPO** spectrum showed four emission bands at approximately 430 nm, 490 nm (shoulder), 550 nm, and 610 nm on a nanosecond timescale after light excitation (Fig. 3a). Two emission bands were also observed at 430 and 490 nm in the **Gd-MCPO** spectrum (Fig. 3b); these bands were assigned to the fluorescence and phosphorescence exhibited by the localized MCPO excited states,

respectively (Fig. S18). These results confirm that the additional emission bands at 550 nm and 610 nm for **Eu-MCPO** are associated with specific Eu(III) orbitals (Fig. 3a). The emission band at 610 nm corresponds to the $^5D_0 \rightarrow {}^7F_2$ transition. Time-resolved emission spectra (Fig. S19) revealed an emission lifetime (τ) of 4.1 ns in the transition at 550 nm, characterized by fluorescence from the septet state (The characteristic emission band at 550 nm is also observed for **Eu-MCPO** excited by 440 nm (Supplementary Note 5, Fig. S33).). This fluorescence band was not observed for **Eu-MCPO-H₂O** (Fig. S20). To determine the origin of the fluorescence band at 550 nm in the spectrum of **Eu-MCPO**, we investigated its structural relaxation in the lowest CT excited state between the 4f- and π-orbitals and associated changes in the electronic transition property using quantum chemical calculations. The calculations indicated that the CT excited state of **Eu-MCPO** would be strongly stabilized by structural relaxation after the transition from the ground state (Fig. S21). Transition orbital analysis of the structure with large oscillator strength during structural relaxation confirmed that the emissive transition originated from the CT excited states between the 4f- and π-orbitals (Fig. 3c). To reveal the excited state dynamics related to the CT excited state between the 4f and π-orbitals, we used kinetic analysis to estimate the energy transfer rate constants (k_{EnT}) from 4f-4f to the CT excited state. The temperature dependence of k_{EnT} was expected to follow an Arrhenius-type equation:

$$\ln\left(\frac{1}{\tau_{obs}} - \frac{1}{\tau_{const}}\right) = ln(k_{EnT}) = lnA - \frac{E_a}{R} \times T^{-1}$$

where A and E_a denote the frequency factor and activation energy, respectively. According to the temperature-dependent emission lifetime (Fig. S23), the activation energy is estimated to be 740 cm⁻¹. The sum of the $^5D_0$ energy level and E_a is 17,990 cm⁻¹, which is similar in energy to the CT excited state. Arrhenius analyses suggested an energy migration channel between $^5D_0$ and the CT excited state (depicted in the energy diagram shown in Fig. 4). Based on the experimental findings and theoretical analyses, the observed emission at around 550 nm is conclusively attributed to transition from the 4f- to π-orbital in a Eu(III) complex.

To obtain a more detailed understanding of excited-state dynamics for **Eu-MCPO**, we calculated the energy transfer rate constants from the MCPO to the Eu(III) ion using LUMPAC software (the detail procedure is summarized in Supplementary Note 2)[27]. The calculated energy transfer rates from T₁ to $^5D_1$ and from T₁ to $^5D_0$ are 6.5×10^8 and $5.9 \times 10^8 \, s^{-1}$, respectively. The T₁ → S₀ deactivation rate was experimentally estimated to be $2.2 \, s^{-1}$ at 100 K using **Gd-MCPO** (Fig. S24), which is significantly lower than the calculated energy transfer rate. The observed phosphorescence at 490 nm in the nanosecond range for **Eu-MCPO** (Fig. 3a) is extremely weak, which reveals that the CT emission is also extremely weak. This relatively low emission intensity is caused by small radiative and large non-radiative rate constants. The small radiative rate constant induced by the phosphine oxide spacer was also confirmed in the CT excited state (Fig. S22). The large non-radiative rate constant is related to the drastic excited energy level changes in the CT excited states. Based on these photophysical findings and theoretical considerations, it is evident that designing an Eu(III) complex with donor-type ligands that strongly overlap with the 4f-orbital and provide a rigid structure is crucial for achieving strong CT emissions from 4f- to π-orbitals.

Conclusion
In summary, the CT emission from 4f- to π-orbitals in the solid-state Eu(III) complex was demonstrated using time-resolved emission spectroscopy. The observed CT emission underwent a nanosecond-scale fast decay, indicating the occurrence of fluorescence from the septet states. Quantum chemical calculations revealed the contribution of CT transitions, energy variability within the CT excited states, and slight mixing between the π- and 4f-orbitals. The small radiative rate constant and large non-radiative rate constant, as predicted by electronic absorption and quantum chemical calculations, resulted in weak emission intensity. Based on these

photophysical and theoretical findings, it is evident that designing donor-type ligands that strongly overlap with the 4f-orbital and provide a rigid structure is crucial for achieving strong CT emissions from 4f- to π-orbitals. The effective use of CT excitons based on the 4f-orbital provides new insights into the design of next-generation nanomaterials and promotes the development of a research domain within the field of light science and technology.

Methods

General methods

NMR spectra were recorded on a JEOL ECS-400 spectrometer ([1]H: 400 MHz, [13]C: 100 MHz, [31]P: 162 MHz). Tetramethylsilane ($\delta = 0.00$ ppm for ^{1}H NMR), CDCl$_3$ ($\delta = 77.0$ ppm for ^{13}C NMR), and H$_3$PO$_4$ ($\delta = 0.00$ ppm for ^{31}P NMR) were employed as internal standards. Electrospray ionization (ESI) mass spectrometry was performed using JEOL JMS-T100 LP instrument. Elemental analyses were performed using MICRO CORDER JM10. Fourier transform infrared (FT-IR) spectra were recorded on a JASCO FT/IR-4600 spectrometer. Thermogravimetry (TG) analysis was performed on a Seiko Instruments Inc. EXSTAR 6000 (TG/DTA6300) under a nitrogen atmosphere at a heating rate of 5 °C min^{-1}. Cyclic voltammetry experiments were conducted using a BAS Model 2325 electrochemical apparatus.

Optical measurements

Diffuse reflection spectra were obtained using a JASCO V-670 spectrophotometer with an ISN-723 integrating sphere unit. Steady-state emission spectroscopy for solid-state Eu(III) and Gd(III) complexes was conducted using a Horiba Fluorolog-3 spectrofluorometer equipped with a cryostat (Thermal Block Company, SA-SB1905HA). The delayed emission spectrum for the solid-state Gd(III) complex was recorded on an FP-6300 spectrofluorometer with a cryostat (Thermal Block Company, SA-SB1905HA). Time-resolved emission spectroscopy for the evaluation of solid-state Eu(III) and Gd(III) complexes was performed on an optical setup consisting of Ti : Sapphire solid-state laser with an optical parametric oscillator (OPO), a 3D Raman confocal microscope system, a high-resolution monochromator, and a streak camera. The particle was directly dispersed on a copper substrate. It was excited with an OPO (Chameleon Vision-S, Coherent, Inc.) pumped by a pulsed Ti:Sapphire laser with an emission wavelength at 365 nm, which is able to generate the SHG laser beam at 730 nm with 75 fs pulse width and 2 MHz repetition rate. The 3D Raman confocal microscope system (Nanofinder 30, Tokyo Instruments, Inc.) functions as a real-time imaging spectrometer to monitor the emission from single-particle phosphors under the OPO laser excitation. The reflected optical signals, collected through a fluorescence microscope (BX51M, Olympus Co., Ltd.) was directed to a high-resolution monochromator (SpectraPro HRS-300, Princeton Instruments, Inc.) and a streak camera (C14831-110, Hamamatsu Photonics Co., Ltd.). The emission spectral range was monitored between 406 nm and 730 nm with a 40 g mm^{-1} grating. The measurement timescale was set to 50 ns, and low temperature experiments (100 K) were performed in a microscopy cryostat (Janis ST-500, Lake Shore Cryotronics, Inc.). Temperature-dependent 4f-4f emission lifetimes for **Eu-MCPO** were measured using the third harmonic (λ_{ex} = 355 nm) of a Q-switched Nd:YAG laser (Spectra Physics, INDI-50, fwhm = 5 ns, λ = 1064 nm) and a photomultiplier (Hamamatsu Photonics, R5108, response time ≤1.1 ns) with a cryostat (Thermal Block Company SA-SB245T) and a temperature controller (Scientific Instruments Model 9700).

Materials

Europium(III) nitrate hexahydrate, 3N5, gadolinium nitrate hexahydrate, 3N5, *n*-butyllithium (*n*-BuLi) in *n*-hexane (1.6 mol/L), and chloroform-*d* (99.8%) were purchased from Kanto Chemical Co., Inc. Dichloromethane (for organic synthesis), methanol, super dehydrated (for organic synthesis), tetrahydrofuran, super dehydrated, with a stabilizer (for organic synthesis), hydrogen peroxide (30%), and sodium sulfate, anhydrous were purchased from Wako Pure Chemical Industries, Ltd. 3,6-Dimethoxy-9H-carbazole (>98.0%) and chlorodiphenylphosphine (>97.0%) were purchased from Tokyo Chemical Industry Co., Ltd.

Preparation of (3,6-dimethoxy-9H-carbazol-9-yl)diphenylphosphine oxide (MCPO).

MCPO was synthesized by a previously reported method. 3,6-Dimethoxy-9H-carbazole (1.0 g, 4.4 mmol) was dissolved in anhydrous THF (30 mL) under argon. *n*-BuLi (5.0 mL, 7.8 mmol) was added slowly dropwise to the solution at −78 °C and stirred for 3 h. Then PPh$_2$Cl (1.5 mL, 8.4 mmol) was added at −78 °C and stirred for 18 h. The product was extracted using CH$_2$Cl$_2$, and the extract was washed with water. The extract was dried over anhydrous Na$_2$SO$_4$ and concentrated by a rotary evaporator. The reaction mixture was dissolved in CH$_2$Cl$_2$ (10 mL) and the solution was cooled at 0 °C. A 30% hydrogen peroxide aqueous solution (7.5 mL) was added to the solution, and the reaction mixture was stirred for 4 h. The product was extracted using CH$_2$Cl$_2$, and the extract was washed with water. The extract was dried over anhydrous Na$_2$SO$_4$ and the solution was evaporated. The product was purified by silica gel chromatography (3% CH$_2$Cl$_2$-MeOH). A white powder was obtained by reprecipitation using CH$_2$Cl$_2$-hexane.

Yield: 879.6 mg (47%). ^{1}H NMR (400 MHz, CDCl$_3$, Fig. S2) δ/ppm = 7.75–7.68 (m, 4H), 7.61 (td, J = 7.3, 1.4 Hz, 2H), 7.47 (td, J = 7.5, 3.4 Hz, 4H), 7.42 (d, J = 2.4 Hz, 1H), 7.15 (d, J = 9.1 Hz, 2H), 6.80 (dd, J = 9.1, 2.4 Hz, 2H), 3.88 (s, 3H). ^{13}C NMR (100 MHz, CDCl$_3$, Fig. S3) δ/ppm = 155.1, 136.7, 133.1, 132.0, 130.3, 128.9, 127.2, 115.8, 114.8, 102.7, 55.8. ^{31}P NMR (162 MHz, CDCl$_3$, Fig. S4) d/ppm = 25.9 (s). FT-IR $\bar{\nu}$/cm^{-1} = 1196 (s, P = O). MS (ESI): m/z calcd for C$_{26}$H$_{23}$NO$_3$P [M + H]$^+$ = 428.14; found: 428.14. Elemental analysis calc. (%) for [C$_{26}$H$_{22}$NO$_3$P]: C 73.06, H 5.19, N 3.28; found: C 72.70, H 5.13, N 3.22.

Preparation of Eu(NO$_3$)$_3$(MCPO)(H$_2$O) (Eu-MCPO-H$_2$O).

MeOH solution (5 mL) containing Eu(NO$_3$)$_3$·6H$_2$O (625.0 mg, 1.401 mmol) and MCPO (298.4 mg, 0.6981 mmol) was stirred for 2 h. The solution was evaporated, and recrystallization in CH$_3$OH gave colorless crystals. Yield: 270.5 mg (32%).

FT-IR $\bar{\nu}$/cm^{-1} = 3116-3681 (st, O–H), 1158 (st, P=O). Elemental analysis calc. (%) for [C$_{52}$H$_{46}$EuN$_5$O$_{16}$P$_2$]: C 51.58, H 3.83, N 5.78; found: C 51.28, H 3.66, N 5.64.

Preparation of Eu(NO$_3$)$_3$(MCPO) (Eu-MCPO).

Eu-MCPO was prepared from **Eu-MCPO-H$_2$O** by heat treatment (400 K, 1 h) under vacuum condition. The elimination of the coordination water was confirmed by thermogravimetric analysis (Fig. S5).

FT-IR $\bar{\nu}$/cm^{-1} = 1149 (st, P=O). Elemental analysis calc. (%) for [C$_{52}$H$_{44}$EuN$_5$O$_{15}$P$_2$]: C 52.36, H 3.72, N 5.87; found: C 51.90, H 3.63, N 5.74.

Preparation of Gd(NO$_3$)$_3$(MCPO)(H$_2$O) (Gd-MCPO-H$_2$O).

MeOH solution (4 mL) containing Gd(NO$_3$)$_3$·6H$_2$O (430.0 mg, 0.9527 mmol) and MCPO (199.8 mg, 0.4674 mmol) was stirred for 2 h. The solution was evaporated, and recrystallization in CH$_3$OH gave colorless crystals. Yield: 164.7 mg (29%).

FT-IR $\bar{\nu}$/cm^{-1} = 3122–3696 (st, O–H), 1162 (st, P=O). Elemental analysis calc. (%) for [C$_{52}$H$_{46}$GdN$_5$O$_{16}$P$_2$]: C 51.36, H 3.81, N 5.76; found: C 50.84, H 3.63, N 5.63.

Preparation of Gd(NO$_3$)$_3$(MCPO) (Gd-MCPO).

Gd-MCPO was prepared from **Gd-MCPO-H$_2$O** according to the same procedure of preparation of **Eu-MCPO**.

FT-IR $\bar{\nu}$/cm^{-1} = 1152 (st, P=O). Elemental analysis calc. (%) for [C$_{52}$H$_{44}$GdN$_5$O$_{15}$P$_2$]: C 52.13, H 3.70, N 5.85; found: C 51.65, H 3.61, N 5.69.

Crystal structure determinations.

The X-ray crystal structures of **Eu-MCPO-H$_2$O** is shown in Fig. S6. The crystallographic data are shown in Table S1. Single crystal X-ray diffraction data were obtained using a

Rigaku XtaLAB Synergy-DW equipped with a HyPix-6000HE detector (MoK$_\alpha$ radiation, $\lambda = 0.71073$ Å). Non-hydrogen atoms were refined anisotropically using the SHELX system. Hydrogen atoms were refined using the riding model. All calculations were performed using the crystal structure crystallographic and Olex 2 software package. The CIF data were confirmed by the check CIF/PLATON service. CCDC-2324703 (for **Eu-MCPO-H$_2$O**) contain the supplementary crystallographic data for this paper. These data can be obtained free of charge from The Cambridge Crystallographic Data Centre via www.ccdc.cam.ac.uk/data_request/cif. Powder X-ray diffractometry (PXRD) was performed on a Rigaku SmartLab using Cu K$_\alpha$ radiation ($\lambda = 1.5418$ Å).

Data availability
The single-crystal data generated in this study have been deposited in The Cambridge Crystallographic Data Center under accession code CCDC-2324703 (Supplementary Data 1). The data can be obtained free of charge from The Cambridge Crystallographic Data Centre via www.ccdc.cam.ac.uk/structures. The atomic coordinates for calculated structures (Figs. S8 and S15) can be obtained from Supplementary Data 2. All of the other data supporting the findings of this study are available from the corresponding author upon reasonable request.

Abbreviations
CT   charge transfer.
LMCT   ligand-to-metal charge transfer.
MLCT   metal-to-ligand charge transfer.

References
1. Kinoshita, T. Highly efficient wideband solar energy conversion employing singlet-triplet transitions. *Bull. Chem. Soc. Jpn.* **95**, 341–352 (2022).
2. Yamazaki, Y., Takeda, H. & Ishitani, O. Photocatalytic reduction of CO_2 using metal complexes. *J. Photochem. Photobiol., C* **25**, 106–137 (2015).
3. Lo, K. W., Tong, G. S. M., Cheng, G., Low, K. H. & Che, C. M. Dinuclear Pt^{II} complexes with strong blue phosphorescence for operationally stable organic light-emitting diodes with EQE up to 23% at 1000 cd m^{-2}. *Angew. Chem., Int. Ed.* **61**, e202115515 (2022).
4. Wegeberg, C., Häussinger, D. & Wenger, O. S. Pyrene-decoration of a Chromium(0) tris(diisocyanide) enhances excited state delocalization: A strategy to improve the photoluminescence of 3d^6 metal complexes. *J. Am. Chem. Soc.* **143**, 15800–15811 (2021).
5. Bürgin, T. H., Glaser, F. & Wenger, O. S. Shedding light on the oxidizing properties of spin-flip excited states in a Cr(III) polypyridine complex and their use in photoredox catalysis. *J. Am. Chem. Soc.* **144**, 14181–14194 (2022).
6. Woodhouse, M. D. & McCusker, J. K. Mechanistic origin of photoredox catalysis involving Iron(II) polypyridyl chromophores. *J. Am. Chem. Soc.* **142**, 16229–16233 (2020).
7. Kinoshita, T. et al. Enhancement of near-IR photoelectric conversion in dye-sensitized solar cells using an osmium sensitizer with strong spin-forbidden transition. *J. Phys. Chem. Lett.* **3**, 394–398 (2012).
8. Steube, J. et al. Janus-type emission from a cyclometalated iron(III) complex. *Nat. Chem.* **15**, 468–474 (2023).
9. Zhang, Y. et al. Delayed fluorescence from a zirconium(IV) photosensitizer with ligand-to-metal charge-transfer excited states. *Nat. Chem.* **12**, 345–352 (2020).
10. Jørgensen, C. K. Electron transfer spectra of lanthanide complexes. *Mol. Phys.* **5**, 271–277 (1962).
11. Bünzli, J.-C. G. Benefiting from the unique properties of lanthanide ions. *Acc. Chem. Res.* **39**, 53–61 (2006).
12. Kitagawa, Y., da Rosa, P. P. F. & Hasegawa, Y. Charge-transfer excited states of π- and 4f-orbitals for development of luminescent. *Dalton Trans.* **50**, 14978–14984 (2021).
13. Tsaryuk, V. I., Zhuravlev, K. P. & Gawryszewska, P. Processes of luminescence quenching in europium aromatic carboxylates with the participation of LMCT states: a brief review. *Coord. Chem. Rev.* **489**, 215206 (2022).
14. Napier, G. D. R., Neilson, R. J. D. & Shepherd, T. M. Charge-transfer excited state in tris(acetylacetonato) europium(III). *Chem. Phys. Lett.* **31**, 328–330 (1975).
15. Berry, M. T., May, P. S. & Xu, H. Temperature dependence of the Eu^{3+} $^5D_0$ lifetime in europium tris(2,2,6,6-tetramethyl-3,5-heptanedionato). *J. Phys. Chem.* **100**, 9216–9222 (1996).
16. Villata, L. S., Wolcan, E., Féliz, M. R. & Capparelli, A. L. Competition between intraligand triplet excited state and LMCT on the thermal quenching in β-diketonate complexes of Europium(III). *J. Phys. Chem. A* **103**, 5661–5666 (1999).
17. Gawryszewska, P. et al. Experimental and theoretical study of the photophysics and structures of europium cryptates incorporating 3,3'-bi-isoquinoline-2,2'-dioxide. *ChemPhysChem* **5**, 1577–1584 (2004).
18. Faustino, W. M., Malta, O. L. & de Sá, G. F. Intramolecular energy transfer through charge transfer state in lanthanide compounds: a theoretical approach. *J. Chem. Phys.* **122**, 054109 (2005).
19. Fu, L. M. et al. Role of ligand-to-metal charge transfer state in nontriplet photosensitization of luminescent europium complex. *J. Phys. Chem. A* **114**, 4494–4500 (2010).
20. Räsänen, M. et al. Study on photophysical properties of Eu(III) complexes with aromatic β-diketones—role of charge transfer states in the energy migration. *J. Lumin.* **146**, 211–217 (2014).
21. Miranda, Y. C. et al. The role of the ligand-to-metal charge-transfer state in the dipivaloylmethanate-lanthanide intramolecular energy transfer process. *Eur. J. Inorg. Chem.* **18**, 3019–3027 (2015).
22. Nonat, A. et al. The role of ligand to metal charge-transfer states on the luminescence of Europium complexes with 18-membered macrocyclic ligands. *Dalton Trans.* **48**, 4035–4045 (2019).
23. Kitagawa, Y., Kumagai, M., da Rosa, P. P. F., Fushimi, K. & Hasegawa, Y. Long-range LMCT coupling in Eu^{III} coordination polymers for an effective molecular luminescent thermometer. *Chem. – Eur. J.* **27**, 264–269 (2021).
24. da Rosa, P. P. F. et al. Coordination geometrical effect on ligand-to-metal charge transfer-dependent energy transfer processes of luminescent Eu(III) complexes. *J. Phys. Chem. A* **125**, 209–217 (2021).
25. Tsurui, M. et al. Asymmetric lumino-transformer: circularly polarized luminescence of chiral Eu(III) coordination polymer with phase-transition behavior. *J. Phys. Chem. B* **126**, 3799–3807 (2022).
26. Faustino, W. M. et al. Photoluminescence of europium(III) dithiocarbamate complexes: electronic structure, charge transfer and energy transfer. *J. Phys. Chem. A* **110**, 2510–2516 (2006).
27. Dutra, J. D. L., Bispo, T. D. & Freire, R. O. LUMPAC Lanthanide luminescence software: efficient and user friendly. *J. Comput. Chem.* **35**, 772–775 (2014).

Author contributions

Competing interests

The authors declare no competing interests.

Additional information

Supplementary information The online version contains supplementary material available at https://doi.org/10.1038/s42004-025-01420-6.

Correspondence and requests for materials should be addressed to Yuichi Kitagawa or Yasuchika Hasegawa.

Peer review information *Communications Chemistry* thanks Jean-Claude Bünzli and the other, anonymous, reviewers for their contribution to the peer review of this work. Peer reviewer reports are available.

Reprints and permissions information is available at http://www.nature.com/reprints

Publisher's note Springer Nature remains neutral with regard to jurisdictional claims in published maps and institutional affiliations.